Analysis and Optimization of a Novel Brushless Compound-Structure Permanent-Magnet Synchronous Machine

Ping Zheng, *Senior Member, IEEE*, Qian Wu, Jingang Bai, Wei Shi, Yi Sui
Department of Electrical Engineering, Harbin Institute of Technology, Harbin 150080, China
zhengping@hit.edu.cn

***Abstract*-A novel brushless compound-structure permanent-magnet synchronous machine (CS-PMSM) is proposed in this paper. The structural characteristics are described and the operation principle is introduced. The equivalent magnetic circuit of the BDRM is established, and the electromagnetic torque is deduced by analytical method. The new type of brushless CS-PMSM consists of one stator machine (SM) and one brushless double rotor machine (BDRM). Using 3D finite element method (FEM), a BDRM prototype is designed and evaluated. Some characteristics including air gap flux density, no-load flux linkage, back-EMF, and torque behavior are obtained.**

***Index Terms*-Brushless, compound-structure permanent-magnet synchronous machine (CS-PMSM), analytical method, finite element method (FEM).**

I. INTRODUCTION

Compound-Structure permanent-magnet synchronous machine (CS-PMSM), which is composed of two electric machines, is suitable for hybrid electric vehicles (HEVs). This kind of machine can keep the internal combustion engine (ICE) operating at maximum efficiency by harmonizing its two motors during all driving cycles in HEV, and the drive system with it can be competitive and ideal due to its compact structure and high efficiency [1]-[4].

In the most common structures, brushes and slip rings are essential. It causes a lot of problems, such as maintenance, the friction losses, and so on, which is also the main disadvantage of this kind of machine [5]. Some researches have been done to solve this problem and a novel brushless scheme is proposed in this paper. It consists of one stator machine (SM) and one brushless double rotor machine (BDRM), as shown in Fig. 1.

This paper refers to the analysis of the BDRM performances, by means of analytical method and 3D finite element method (FEM). The equivalent magnetic circuit of the BDRM is analyzed and a BDRM prototype is designed and evaluated using 3D FEM.

II. BASIC TOPOLOGY AND OPERATING PRINCIPLE

The BDRM is a new type 3-phase claw-pole machine with two air gaps and it is composed by three parts: stator 1, claw-pole rotor and permanent-magnet rotor 1. These circumferential coils on stator 1 produce magnetic flux which propagates axially through the stator core down to the side part and then cross the outer air gap into the top of the claw. Thereafter the magnetic flux crosses the inner air gap from the claw foot into one magnet and then circumferentially goes through the permanent-magnet rotor 1 back to the next magnet and once again crosses the inner air gap into the next claw and back through the top of the claw, across the outer air gap and into the next side part. The flux has now traveled around a closed loop linking the winding and the active parts of the machine. Fig. 2 shows the flux path for one pole, the arrow stands for the flux direction.

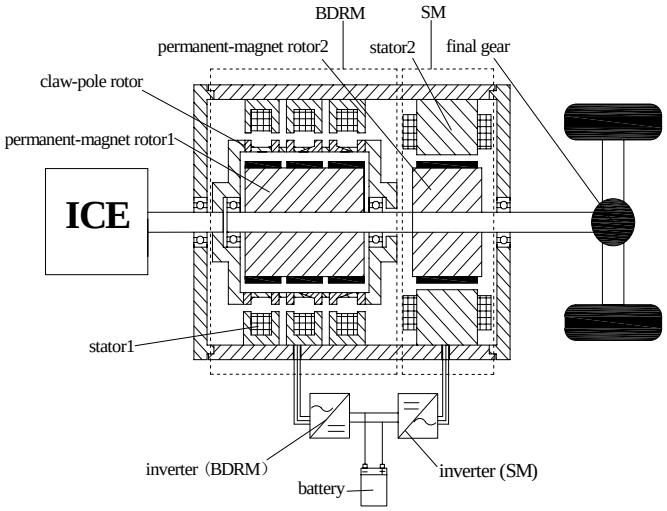

Fig. 1. Brushless CS-PMSM system.

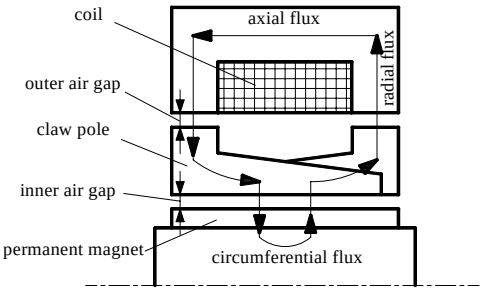

Fig. 2. Flux path in the BDRM.

Arranging three phases coaxially, a three-phase BDRM can be realized by circumferentially shifting the claws 120 electrical degrees, as shown in Fig. 3. In the brushless CS-PMSM system, the claw-pole rotor is connected to the ICE, and the permanent-magnet rotor 1 is connected to the load. Since the claw-pole rotor and permanent-magnet rotor 1 can

978-1-4244-8218-4/10/$26.00 ©2010 IEEE

operate at different speeds, the ICE can operate at the optimum speed independent of the load, so the speed control can be realized. BDRM transfers the ICE torque directly to the load, and SM adds/subtracts additional torque to/from the load, so the torque control can be realized [6]. Thus the BDRM can realize the speed adjustment for power-split HEV use.

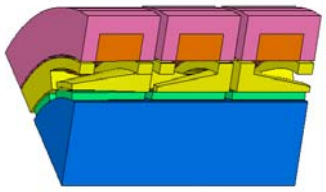

Fig. 3. Three-phase BDRM model.

III. Magnetic Circuit Model and Electromagnetic Torque of the BDRM

The magnetic circuit model is very important for the qualitative analysis and quantitative calculation of electric machine. Due to the complex structure and 3-D magnetic flux path of the claw-pole rotor, the magnetic circuit of the BDRM is much more complicated than conventional machines. The no-load equivalent magnetic circuit of the BDRM has been built as shown in Fig.4.

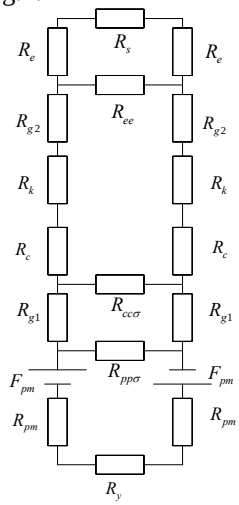

Fig. 4. No-load equivalent magnetic circuit of the BDRM.

where R_y is the yoke reluctance of permanent-magnet rotor 1, R_{pm} is the equivalent inner reluctance of the permanent magnet, F_{pm} is the equivalent magneto motive force (MMF) of the permanent magnet, R_{g1}, R_{g2} are the inner and outer air gap reluctances, R_c is the reluctance of the claw pole, R_k is the reluctance of the knee which connects different claws, R_e is the stator core end reluctance, R_s is the stator core yoke reluctance, $R_{pp\sigma}$ represents the leakage reluctance between permanent magnets, $R_{cc\sigma}$ and R_{ee} respectively represent the leakage reluctance between the claw poles and between the stator core ends.

The equivalent external magnetic circuit reluctance is

$$\sum R_M = \frac{R_{pp\sigma}(R_b + 2R_{g2})}{R_{pp\sigma} + R_b + 2R_{g2}} + 2R_{pm} + R_y. \tag{1}$$

Where $R_b = \dfrac{R_{cc\sigma}(R_a + 2R_{g1} + 2R_k + 2R_c)}{R_{cc\sigma} + R_a + 2R_{g1} + 2R_k + 2R_c}$,

$$R_a = \frac{R_{ee}(R_s + 2R_e)}{R_{ee} + R_s + 2R_e}.$$

Inner air gap flux:

$$\Phi_{g1} = \frac{2F_M \bullet R_{pp\sigma}}{\left[\dfrac{R_{pp\sigma}(R_b + 2R_{g2})}{R_{pp\sigma} + R_b + 2R_{g2}} + 2R_{pm} + R_y\right]\left(R_b + 2R_{g2} + R_{pp\sigma}\right)} \tag{2}$$

Outer air gap flux:

$$\Phi_{g2} = \frac{\Phi_{g1} \bullet R_{cc\sigma}}{R_a + 2R_{g1} + 2R_k + 2R_c + R_{cc\sigma}} \tag{3}$$

Compared with magnetic circuit of traditional claw-pole permanent-magnet machines [7]-[9], the BDRM has one more air gap and similar flux leakage paths. Additional air gap will decrease the air-gap flux density and torque. In order to maintain the normal air-gap flux, the main magnetic circuit reluctance should be minimized, and leakage reluctance should be maximized, while the MMF of permanent magnets needs to be appropriately raised.

Similarly, the *d*- and *q*-axis equivalent magnetic circuit diagrams with load are shown in Fig. 5.

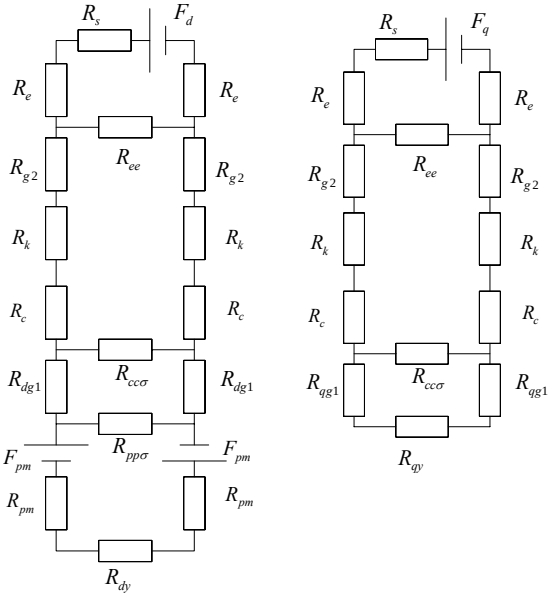

Fig. 5. *D*- and *q*-axis equivalent magnetic circuit diagrams with load. (a) *d* axis; (b) *q* axis.

where R_{dy}, R_{qy} are the *d*- and *q*-axis yoke reluctance of permanent-magnet rotor 1, R_{dg1}, R_{qg1} are the *d*- and *q*-axis inner air gap reluctances, F_d, F_q are the *d*- and *q*-axis armature MMF.

For *d*-axis equivalent magnetic circuit:

Inner air gap flux produced by the permanent magnets is

$$\Phi_{pm\delta 1}=\frac{2F_{pm}\bullet R_{pp\sigma}}{\left[\frac{R_{pp\sigma}(R_b+2R_{dg1})}{R_{pp\sigma}+R_b+2R_{dg1}}+2R_{pm}+R_{dy}\right]\left(R_b+2R_{dg1}+R_{pp\sigma}\right)}. \quad (4)$$

Outer air gap flux produced by the permanent magnets is

$$\Phi_{pm\delta 2}=\frac{\Phi_{pm\delta 1}\bullet R_{cc\sigma}}{R_a+2R_{g2}+2R_k+2R_c+R_{cc\sigma}}. \quad (5)$$

Outer air gap flux produced by *d*-axis armature MMF is

$$\Phi_{id\delta 2}=\frac{F_d\bullet R_{ee}}{\left[\frac{R_{ee}(R_n+2R_{g2}+2R_k+2R_c)}{R_{ee}+R_n+2R_{g2}+2R_k+2R_c}+2R_e+R_s\right]\left(R_n+2R_{g2}+2R_k+2R_c+R_{ee}\right)}. \quad (6)$$

Where, $R_n=\frac{R_{cc\sigma}(R_m+2R_{dg1})}{R_{cc\sigma}+R_m+2R_{dg1}}$,

$$R_m=\frac{R_{pp\sigma}(R_{dy}+2R_{pm})}{R_{pp\sigma}+R_{dy}+2R_{pm}}.$$

Inner air gap flux produced by *d*-axis armature MMF is

$$\Phi_{id\delta 1}=\frac{\Phi_{id\delta 2}\bullet R_{cc\sigma}}{R_m+2R_{dg1}+R_{cc\sigma}}. \quad (7)$$

The main magnetic flux in inner and outer air gap is

$$\Phi_{d\delta 1}=\Phi_{pm\delta 1}+\Phi_{id\delta 1}, \quad (8)$$

$$\Phi_{d\delta 2}=\Phi_{id\delta 2}+\Phi_{pm\delta 2}. \quad (9)$$

For *q*-axis equivalent-magnetic-circuit:

Outer air gap flux produced by *q*-axis armature MMF is

$$\Phi_{q\delta 2}=\frac{F_q\bullet R_{ee}}{\left[\frac{R_{ee}(R_x+2R_{g2}+2R_k+2R_c)}{R_{ee}+R_x+2R_{g2}+2R_k+2R_c}+2R_e+R_s\right]\left(R_x+2R_{g2}+2R_k+2R_c+R_{ee}\right)}. \quad (10)$$

Where, $R_x=\frac{R_{cc\sigma}(R_{qy}+2R_{qg1})}{R_{cc\sigma}+R_{qy}+2R_{qg1}}$.

Inner air gap flux produced by *q*-axis armature MMF is

$$\Phi_{q\delta 1}=\frac{\Phi_{q\delta 2}\bullet R_{cc\sigma}}{R_{qy}+2R_{qg1}+R_{cc\sigma}}. \quad (11)$$

The final expression of BDRM electromagnetic torque is shown in (12).

$$\begin{aligned}T_{em}&=\frac{mp}{\sqrt{2}}Nk_w(\Phi_{d\delta 1}I_q-\Phi_{q\delta 1}I_d)\\&=\frac{mp}{\sqrt{2}}N(\Phi_{id\delta 1}I_q+\Phi_{pm\delta 1}I_q-\Phi_{q\delta 1}I_d)\\&=\frac{mp}{\sqrt{2}}N\{\frac{F_d\bullet R_{ee}\bullet R_{cc\sigma}\bullet I_q}{\left[\frac{R_{ee}(R_n+2R_{g2}+2R_k+2R_c)}{R_{ee}+R_n+2R_{g2}+2R_k+2R_c}+2R_e+R_s\right]\left(R_n+2R_{g2}+2R_k+2R_c+R_{ee}\right)(R_m+2R_{dg1}+R_{cc\sigma})}\\&+\frac{2F_{pm}\bullet R_{pp\sigma}\bullet I_q}{\left[\frac{R_{pp\sigma}(R_b+2R_{dg1})}{R_{pp\sigma}+R_b+2R_{dg1}}+2R_{pm}+R_{dy}\right]\left(R_b+2R_{dg1}+R_{pp\sigma}\right)}\\&-\frac{F_q\bullet R_{ee}\bullet R_{cc\sigma}\bullet I_d}{\left[\frac{R_{ee}(R_x+2R_{g2}+2R_k+2R_c)}{R_{ee}+R_x+2R_{g2}+2R_k+2R_c}+2R_e+R_s\right]\left(R_x+2R_{g2}+2R_k+2R_c+R_{ee}\right)(R_{qy}+2R_{qg2}+R_{cc\sigma})}\}\end{aligned} \quad (12)$$

where T_{em} is the BDRM electromagnetic torque, m is the phase number, p is the pole-pair number, N is the number of stator-coil turns, k_w is the stator fundamental winding factor, and I_d, I_q are the stator *d*- and *q*-axis armature currents.

IV. 3D Finite Element Analysis of the BDRM

Before designing the BDRM, some cases must be taken into account as the special structure and particular working environment:

1) The BDRM is mainly used for deceleration generator in the system, and the output speed of automobile engine varies greatly from no-load to full-load, so the BDRM should be reliable to generate electricity both at high speed and the low one. This is completely different from usual synchronous generator whose prime mover speed is constant. In order to adapt to the feature of wide speed range, to prevent excessive magnetic circuit saturation, the no-load flux density of the BDRM is selected at a low level.

2) Owing to the double air gaps in the BDRM, the gap length should be minimized to reduce the excitation MMF in the context of maintaining concentricity and dynamic balance of the rotors.

3) The stator core end and yoke thickness can be appropriately increased to expand the outer air gap cross-sectional area, so as to reduce the air gap MMF.

4) Winding resistance and reactance values could be appropriately larger according to the greatly changed speed of generator. When the back-EMF value increases with the increasing speed of the prime mover, the frequency also increases, so that the generator internal impedance increases. These series of changes automatically limit the operating current to avoid burn out generator winding. But the resistance and reactance value should not be too large, resulting in lack of output current.

5) As complex structure of the claw-pole rotor, it is difficult to be made by silicon steel sheet, and if traditional solid steel is used, eddy current and hysteresis losses will be large. Therefore, researchers propose the use of soft magnetic composite (SMC) materials which have advantage of isotropic magnetic propertie for three-dimensional magnetic flux path, complex structure motors. SMC materials are manufactured from iron-powder by coated, insulated partide surfaces, so its eddy current loss is small [10]-[12].

6) The claw-pole rotor can not be directly made integrated. These claws are fixed by mechanical connection of non-magnetic material such as stainless steel or copper filled between the poles.

A 10kW BDRM model has been built. Fig.6 shows the exploded view of one-phase BDRM.

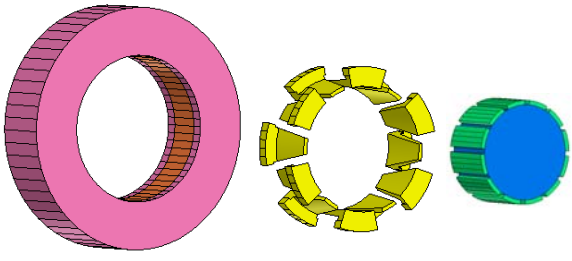

(a) (b) (c)

Fig. 6. Exploded view of one-phase BDRM: (a) stator 1, (b) claw-pole rotor, (c) permanent-magnet rotor 1.

A. Optimization of the BDRM Model

The shape of the claws can adapt to decreasing the harmonic content of the no-load back-EMF and controlling

the amplitude of the cogging torque. The initial claw-pole rotor composed of separate claws is improved by using a knee to connect the separate parts with the same polarity together. Fig. 7 shows the initial claw-pole rotor and improved claw-pole rotor. The improved claw pole rotor is more convenient to keep the claw poles relatively fixed by mechanical connection of non-magnetic material filled between the poles. No-load performance of the BDRM with separate claws and claws connected with a knee is shown in Table I. The results show that the structure of claws connected with a knee has better performance.

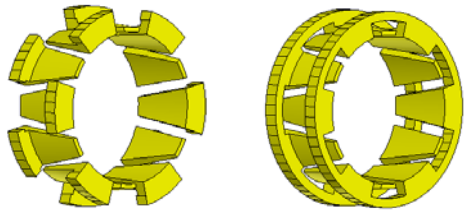

(a) (b)

Fig. 7. The claw-pole rotor: (a) separate claws, (b) claws connected with a knee.

TABLE I
NO-LOAD PERFORMANCE OF THE BDRM WITH SEPARATE CLAWS AND CLAWS CONNECTED WITH A KNEE

	Separate claws	Claws connected with a knee.
Amplitude of fundamental back-EMF (V)	152.65	167.61
THD of back-EMF	4.93%	11.61%
Peak-peak value of cogging torque (N·m)	17	10.5

Different shapes of the claw parts facing the air gap can also be considered. The most common shapes are rectangular, triangular, and trapezoidal [13]. Fig. 8 shows the rectangular shaped claws and the trapezoidal shaped ones. No-load performances of the BDRM with rectangular shaped claws and trapezoidal shaped claws are shown in Table II. The results show that the structure of trapezoidal shaped claws has better performance.

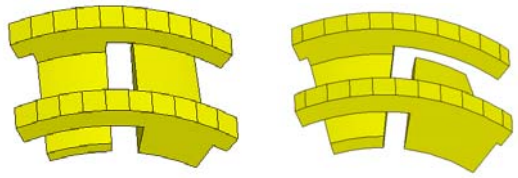

(a) (b)

Fig. 8. The claw-pole rotor: (a) rectangular shaped claws, (b) trapezoidal shaped claws.

TABLE II
NO-LOAD PERFORMANCE OF THE BDRM WITH RECTANGULAR SHAPED CLAWS AND TRAPEZOIDAL SHAPED CLAWS

	Rectangular shaped claws	Trapezoidal shaped claws
Amplitude of fundamental back-EMF (V)	157.1558	167.61
THD of back EMF	19.81%	11.61%
Peak-peak value of cogging torque (N·m)	12	10.5

Fig. 9 and 10 show the effects of air gap length and pole embrace of the permanent magnets on the torque characteristics. It can be seen that the average torque is proportional to the pole embrace of the permanent magnets, and inversely proportional to the air gap length. The practical dimension choice can be made by the torque ripple value and can also be considered according to the specifications and the constraints of the application.

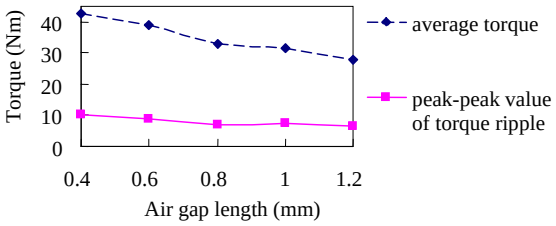

Fig. 9. Effect of air gap length on the torque characteristics.

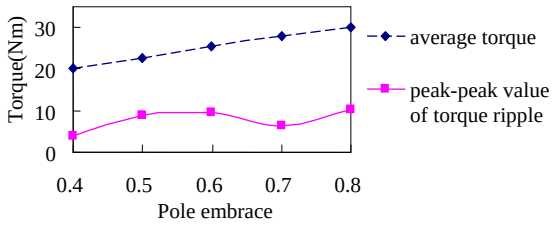

Fig. 10. Effect of the pole embrace of the permanent magnets on the torque characteristics.

B. *Parameter Characteristics of the Optimized BDRM Model*

This section shows the parameter characteristics of the optimized BDRM model. Fig. 11 shows the no-load flux density distribution at maximum linked flux. It can be seen that the density distributed around claw poles is maximum. Fig. 12 shows the flux density distribution in inner and outer air gap along the circumferential direction.

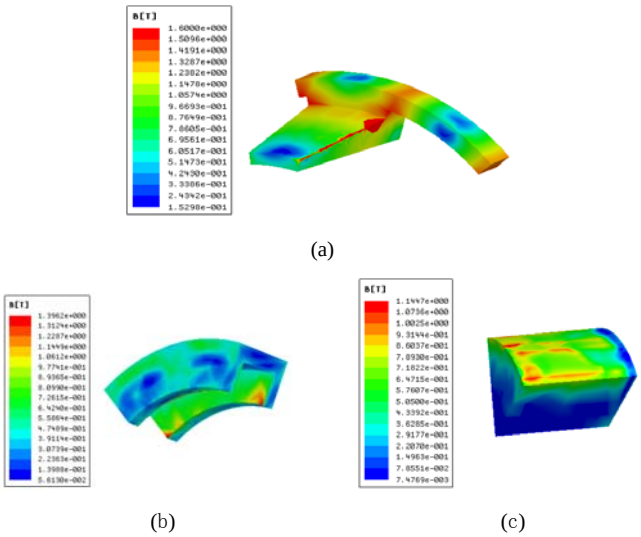

(a)

(b) (c)

Fig. 11. No-load flux density distribution at maximum linked flux: (a) the claw pole, (b) stator core, (c) permanent-magnet rotor core.

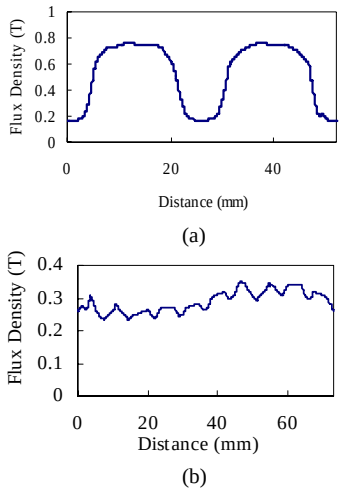

Fig. 12. The distributed plot of air gap magnetic flux density: (a) inner air gap, (b) outer air gap.

Fig. 13 shows the flux-linkage waveforms of three-phase BDRM. The back-EMF curve in Fig. 14 which is similar to sinusoidal one proves a good design of the magnetic structure.

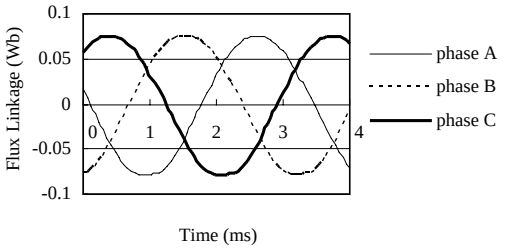

Fig. 13. The flux-linkage waveforms of three-phase BDRM.

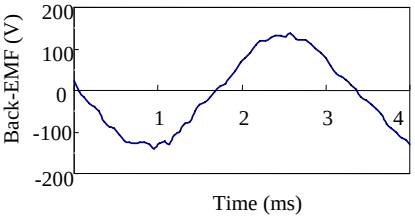

Fig. 14. Back-EMF in one-phase at no-load.

Fig. 15 shows FEM calculated torque curve of the BDRM at rated-load and that the maximum torque ripple is acceptable in the vehicle traction application.

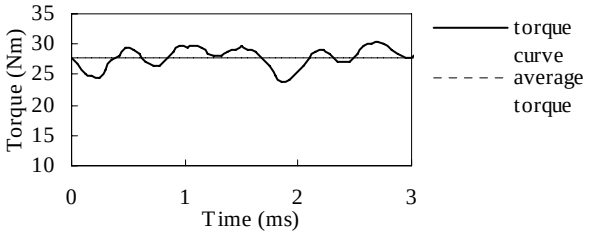

Fig. 15. FEM calculated torque curve of the BDRM.

V. CONCLUSIONS

A new structure of brushless CS-PMSM has been presented. This structure has a great advantage in eliminating the brushes and slip rings in the formal CS-PMSM. The equivalent magnetic circuit of the BDRM is built and the electromagnetic torque formula is deduced. The 3D FEM is used to build and analyze the configuration of the BDRM which is the innovative part in the brushless CS-PMSM. Some characteristics including air gap flux density, no-load flux linkage, back-EMF, and torque behavior are obtained. The new type machine represents a promising solution for HEV drive system. It is expected that more important results and observations will be encountered in the coming years.

ACKNOWLEDGMENT

This work was supported in part by the 863 Plan of China under Project 2006AA05Z231, in part by National Natural Science Foundation of China under Project 50577011, and in part by Program for New Century Excellent Talents in University under Project NCET-06-0347.

REFERENCES

[1] S. Eriksson, and C. Sadarangani, “A four-quadrant HEV drive system,” *Proceedings of Vehicular Technology Conference*, 2002, pp. 1510-1514.

[2] P. Zheng, P. Thelin, A. Y. Chen, and E. Nordlund, “Influence of Saturation and Saliency on the Inductance of a Four-Quadrant Transducer Prototype Machine,” *IEEE Transactions on Magnetics*, 2006, pp. 1319-1322.

[3] R. Liu, P. Zheng, H. Zhao, and C. Sadarangani, “Investigation of a compound-structure permanent-magnet synchronous machine used for HEVs,” *2008 IEEE Vehicle Power and Propulsion Conference*, Harbin, China, 2008, pp. 1-5.

[4] L. Y. Xu, and Y. Zhang, “Design and Evaluation of a Dual Mechanical Port Machine and System,” *Proceedings of the 5th International Power Electronics and Motion Control Conference*, 2006, pp. 1-5.

[5] F. tao, W. Xuhui, X. shan, and K. Liang, “A brushless permanent magnet dual mechanical port machine for hybrid electric vehicle application,” *ICEMS*, Oct, 2008, pp. 3604-3607.

[6] P. Zheng, Nordlund, and Thelin, “Investigation of the winding current distribution in a 4-quadrant-transducer prototype machine,” *IEEE Transactions on Magnetics*, 2005, pp. 973-975.

[7] J. Florin, M. Claudia, and B. Karoly, “Comparative Analysis of the Claw-Pole Rotor Dimensions Influence on the Performances of a Claw-Pole Generator for Wind Applications,” *ICCEP*, Capri, Italy, June, 2009, pp. 715-720.

[8] F. Zhang, Y. Liu, and H. Bai, “Study and design of 3-D flux permanent magnet claw-pole motor with SMC stator,” *Proceedings of 2009 IEEE International Conference on Applied Superconductivity and Electromagnetic Devices*, Chengdu, China, 2009, pp.316-319.

[9] F. Zhang, H. Bai, S. Zhang, H. P. Gruenberger, and E Nolle, “Electromagnetism model and characteristic simulation of novel claw pole generator with permanent magnet outer rotor,” *Power Electronics and Motion Control Conference*, 2006, pp. 1-5.

[10] Y. G. Guo, J. G. Zhu, D. Dorrell, H. Y. Lu, and Y. Wang, “Development of a claw pole permanent magnet motor with a molded low density soft magnetic composite stator core,” *The first IEEE Energy Conversion Congress and Exposition*, California, USA, September, 2009, pp. 20-24.

[11] Y. G. Guo, J. G. Zhu, J. J. Zhong, and W. Wu, “Core losses in claw pole permanent magnet machines with soft magnetic composite stators,” *IEEE Transactions on Magnetics*, vol. 39, no. 5, 2003, pp. 3199-3201.

[12] Y. K. Huang, J. G. Zhu, Y. G. Guo, Z. W. Lin, and Q. S. Hu, “Design and analysis of a high speed claw pole motor with soft magnetic composite core for micro turbine application,” *MMM/Intermag07,* Baltimore, USA, January 2007, pp. 2492-2494.

[13] J. Cros and P. Viarouge, “New Structures of Polyphase Claw-Pole Machines,” *IEEE Transactions on Industry Applications*, vol. 40, January/February 2004, pp.113-120.